

Session III

STELLAR EJECTA AND IMPACT ON EXOPLANETS

Observations of stellar coronae and prominences

Gaitee A. J. Hussain

ESO, Karl-Schwarzschild-Strasse 2, D-85748, Garching bei München
Germany
email: ghussain@eso.org

Abstract. X-ray and EUV observations of young cool stars have shown that their coronae are extremely pressured environments with temperatures and densities that are up to two orders of magnitudes larger than those observed in the solar corona. At the same time rapidly transiting absorption features in optical and UV spectra reveal the presence of large cool, prominence-type complexes that can extend several stellar radii. I will give an overview of our current understanding of coronal structures in cool stars from multi-wavelength observations, detailing their properties and apparent dependence on spectral type. I will also outline future prospects in this field, particularly from observations of stellar coronal environments at radio and sub-mm wavelengths.

Keywords. stars: activity, stars: coronae, stars: circumstellar matter, stars: magnetic fields, X-rays: stars

1. Introduction

Thanks to almost fifteen years of observations from the great X-ray facilities, *Chandra* and *XMM-Newton*, we have gained numerous insights into the properties of stellar coronae. Grating X-ray spectra have enabled the measurement of coronal densities at a range of plasma temperatures while time-resolved studies allow us to place strong constraints on the extents and distribution of the hot, MK, plasma. Multiwavelength observations allow us to gain a more complete picture into the range of sizes of coronal structures, from compact X-ray and EUV flares to cool prominence-like structures that extend out to several stellar radii.

While it is now possible to follow the dynamic flows inside prominences on the Sun and categorise in detail the differences between different types of prominences, stellar coronal observations are of course necessarily limited in terms of spatial resolution. Stellar studies can only measure diagnostics that are integrated over the entire stellar disk. Despite this limitation some clear trends emerge with stars of different spectral types and activity levels. These observations combined with the modelling efforts currently underway to understand coronal environments, (e.g., Vidotto *et al.*, *this volume*) provide us with powerful tools to probe the early history of the Sun, the solar system and their place in a wider context.

2. X-ray/EUV spectra: coronal filling factors

X-ray grating spectra from *Chandra* and *XMM-Newton* encompass the He-like triplets of O, Ne, Mg and Si, which are useful diagnostics of plasma conditions (Gabriel & Jordan 1969). Fig. 1 shows the OVII triplet for an active K-type star. The ratio of the fluxes in the forbidden and intercombination lines are mainly density-sensitive in coronae, while all three lines are used to measure the temperature at which these lines have formed

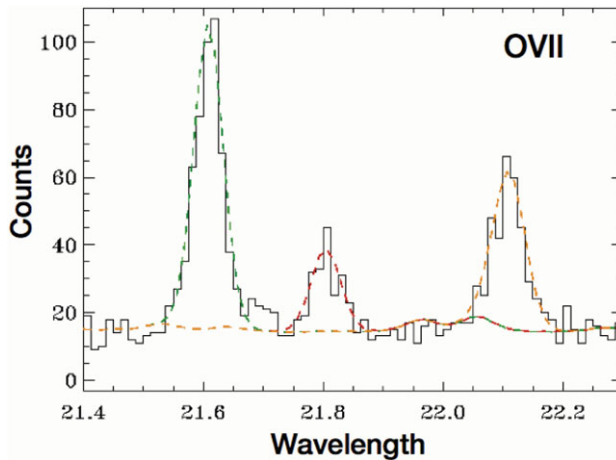


Figure 1. The dashed lines show the fits to the resonance (r : green), intercombination (i : red) and forbidden (f : orange) lines corresponding to the transitions between the $n=2$ shell and $n=1$ ground level in the O VII triplet. The flux ratio between the forbidden and intercombination lines, f/i , is predominantly density-sensitive while the ratio $(f + i)/r$ is temperature-sensitive. Data from Hussain *et al.* (2007).

(see Fig. 1). If we assume isothermal plasma and hydrostatic equilibrium it is possible to compute an upper limit for the filling factor of plasma using the emission measures, density and temperature measurements from these triplets (see Testa *et al.* 2004, Ness *et al.* 2004). While the emission measures and densities imply large coronal volume filling factors compared to the solar corona; the pressure scale heights must be small ($h \ll R_*$).

Coronal densities have been estimated for over 30 G-K-type stars encompassing a range of activity levels and X-ray luminosities ($\log L_X \sim 27-32 \text{ erg s}^{-1}$). Testa *et al.* (2004) focus on the O VII 22Å, and the Mg XI 9Å, He-like triplets that have temperatures of peak formation at a few MK and 10 MK respectively. The lower temperature diagnostic, O VII, indicates typical densities, $n_e \sim 10^{10} - 10^{11} \text{ cm}^{-3}$ in MK plasma, with filling factors ranging from 0.1 in the most inactive stars and increasing to 1.0 in the most rapidly rotating, active stars. This implies that the most active stars are completely covered in dense, MK plasma. The Mg XI diagnostic is sensitive to the hotter, 10 MK plasma, and is therefore associated with the more energetic flares. The observed emission measures and densities from Mg XI yield densities of 10^{12} cm^{-3} and filling factors ranging from 10^{-4} up to 0.1 with increasing activity. This implies that with increasing activity levels, stellar coronae fill up with the type of MK plasma associated with active regions on the Sun until they are essentially completely covered. This rise is accompanied by a corresponding increase in 10 MK plasma at higher densities, with typical $\log n_e \sim 12 \text{ cm}^{-3}$ though the filling factors remain much smaller.

3. X-ray rotational modulation & eclipses

Studies of X-ray rotational modulation in the most active, rapidly rotating stars indicate the presence of compact stable “quiescent” coronal active regions. If observations span several orbital periods, time intervals associated with large energetic flares can be identified and filtered from X-ray and EUV data and enable the study of the quiescent component of the corona. Long X-ray and EUV observations of the contact binaries, 44i Boo and VW Cep, revealed some of the strongest constraints on the locations of coronal active regions (Brickhouse, Dupree & Young 2001, Huenemoerder *et al.* 2003).

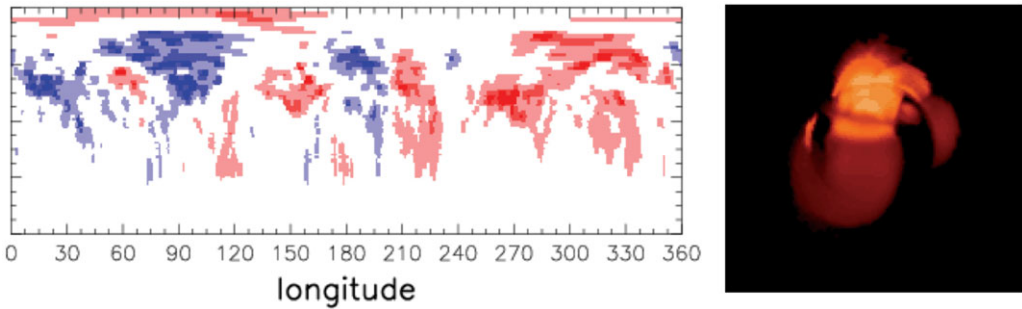


Figure 2. Surface magnetic field map of the K0V star, AB Dor obtained using Zeeman Doppler imaging. This map is a rectangular projection of the stellar surface showing only the radial vector, blue and red represent ± 1 kG respectively. This surface map has been used to model the position of closed corona in the star and therefore to predict the X-ray modulation from the star's X-ray lightcurves from the quiescent active regions (Hussain *et al.* 2007).

Contact binaries are ideally suited to these types of studies as they have relatively short orbital periods ($\ll 1$ d), are X-ray luminous, and show large orbital velocity variations. This means that several orbits can be covered in a short period of time, with sufficient statistics in the X-ray lightcurves to disentangle flaring intervals from quiescent X-ray emission and search robustly for rotational modulation.

Chandra observations of the short period contact binary system 44i Boo (G0V+G0V, $P_{\text{orb}}=0.27$ d) spanning 2.56 orbits show clear modulation in both the X-ray lightcurves and spectra (Brickhouse, Dupree & Young 2001). Modelling of the observed rotational modulation places strong constraints on the extent and distribution of the X-ray emitting active regions. The strongest isolated emission lines (O VIII, Ne X, Fe XVI, Mg XII) show consistent velocity modulations, which closely trace the orbital motion of the primary star. These combined with the 20% X-ray lightcurve modulation indicate that a significant fraction of the coronal X-ray plasma is concentrated on the primary star at high latitudes with a smaller component of emission distributed over both component stars.

The rotation of single and binary stars can also help to measure the sizes and locations of loops associated with large energetic X-ray and EUV flares. In the Algol binary system (B8V+K2IV, $P_{\text{orb}} = 2.86$ d) a strong flare was observed to be completely eclipsed by the primary star, strongly constraining its location to $0.5R_*$ above the “south” pole of the K-star secondary (Schmitt & Favata 1999). This is also consistent with studies of flare heights made from the modelling of flaring loop lengths based on their decay timescales (see Section 4).

3.1. Modelling X-ray coronae from surface magnetic field maps

It is now possible to reconstruct the large scale magnetic field topologies at the surfaces of rapidly rotating cool stars using Zeeman Doppler imaging techniques (Semel 1989, Donati & Collier Cameron 1997, Hussain *et al.* 2000, Kochukhov *et al.* 2013; see Fig. 2). Zeeman Doppler imaging works by inverting a time-series of high resolution circularly polarised spectra obtained from large format optical echelle spectrographs such as CFHT/ESPADONS and the ESO 3.6-m/HARPS instrument in polarimetric mode. The circularly polarised signatures are combined from thousands of photospheric line profiles to detect polarisation signatures down to the 0.1% continuum intensity level. The velocity modulation and amplitude modulation of a time-series of polarisation signatures acquired over a full rotation cycle enable us to identify the position in latitude and longitude and the orientation of the large scale region in velocity and amplitude of

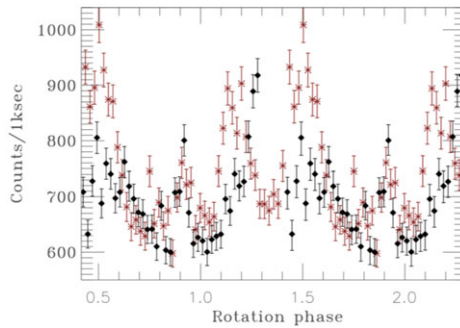


Figure 3. *Chandra* X-ray lightcurve of the active, K0 star, AB Dor covering two consecutive rotation periods with successive cycles marked by black diamonds and red asterisks (from Hussain *et al.* 2007). A period analysis shows significant rotational modulation in the X-ray lightcurve at the 12% level. X-ray models based on contemporaneous surface magnetic field maps of the star can reproduce X-ray emission measures and levels of rotational modulation that are consistent with the observed properties of the star.

these polarisation signatures enable us to identify the field orientation and position of large-scale magnetic field regions at the stellar photosphere.

The surface magnetic field maps from these techniques can be used to model the positions of footpoints of magnetic fields that extend into the corona. This coronal loop model can then be used to model the X-ray corona and predict the location and distribution of coronal active regions. The X-ray corona (e.g., Fig. 2) is modelled using several inputs: (a) the 3-D coronal field model extrapolated from the surface magnetic field map; assuming an isothermal corona with a temperature corresponding to the dominant temperature in its X-ray emission measure distribution (10 MK in the case of the K0 star, AB Dor shown above); (c) assume hydrostatic equilibrium. More details on how the X-ray models are constructed are available in Hussain *et al.* (2007) and references therein.

We find that in order to explain the emission measure, coronal densities and rotational modulation measured in the X-ray lightcurves and spectra (e.g., Fig. 3), and based on the complex multipolar large surface field, AB Dor's corona cannot extend beyond a scale height of $0.3\text{--}0.4R_*$. However, the same dataset indicates that the compact X-ray emitting active regions co-exist with cooler and much larger structures, which subtend several stellar radii and appear to corotate with the star (Section 5).

4. Flaring statistics

Measurements of the flare emission measure and decay timescales can be used to estimate flaring properties including: the temperature, the density and the size of the loop length in which the flare originated. With the archived data from the EUVE satellite it is possible to analyse a large sample of EUV flares on a range of stars consistently (e.g., Mullan *et al.* 2006). They employ the Haisch Simplified Approach which assumes that radiative losses in the earliest decay phases are dominated by bremsstrahlung emission and requires few further assumptions to derive consistent properties over the entire sample. While there are clearly some limitations to this approach, by applying the same technique to a homogeneous dataset it is possible to make a comparative study of the flare properties across a wide range of stars.

From studies of over 100 flares on 33 stars Mullan *et al.* (2006) find clear trends with spectral type (see Fig. 4). There appears to be a transition in the flare loop lengths from compact heights of $L < 0.5R_*$ in the hotter stars, to a range of heights up to $1.5R_*$ in

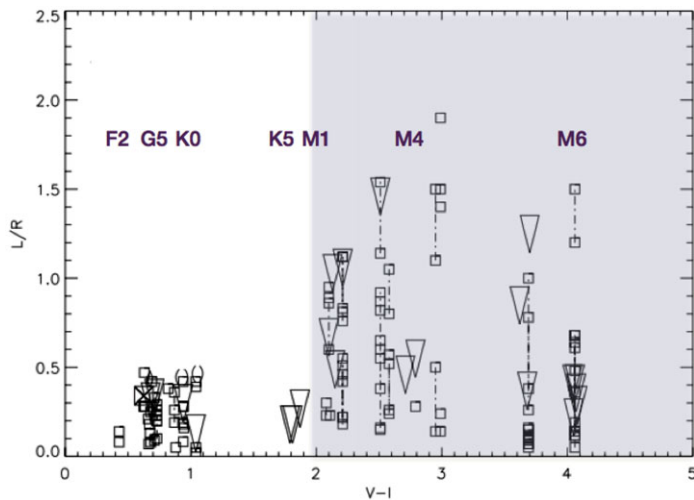


Figure 4. Flaring loop length in 33 main sequence stars derived from EUVE data. The loop length as a fraction of the radius is plotted against $(V-I)$. The corresponding spectral types are denoted along the top. The point at which loop lengths appear to be systematically larger beyond a spectral type of M4 ($V-I \geq 2.7$) (Mullan *et al.* 2006, reproduced by permission of the AAS).

the cooler K2-M0 stars. It is unclear why the transition in loop sizes occurs and similar transitions are not clear in other diagnostics.

Lightcurves are now available that are more sensitive than ever before in “white-light” and cover much longer timescales thanks to high sensitivity photometry obtained from missions such as *Kepler* and *COROT*. Flares detected serendipitously in wide field studies indicate that energetic flares, hitherto supposed to be the domain of the most rapidly rotating cool stars, are also found in relatively slow rotators (Maehara *et al.* 2012, Shibata *et al. this volume*). Follow-up studies are being carried out that aim at characterising these stars in more detail; it remains to be seen whether similar trends with spectral type are found in these ‘white-light’ flares.

5. Stellar prominences

Several stars show evidence of extended structures; these were first detected as fast-moving absorption transient features that move through the $H\alpha$ line profile revealing the presence of cool (10^4K) material subtended out to $5 R_*$, i.e. at and beyond the Keplerian co-rotation radius of the star (Collier Cameron & Robinson 1989). These have been found on almost all rapidly rotating cool stars where dense time-series spectra have been obtained, ranging from G to M-type systems (e.g., Jeffries 1993, Byrne, Eibe & Rolleston 1996, Barnes *et al.* 1998). Up to 7 clouds can be found to exist at any one time, with the number changing from night to night. There is also a hint that some stars host much smaller prominences than others even with similar spectral types (e.g., Barnes *et al.* 1998) though this has not been examined in detail.

The masses of these prominences can be estimated if a number of different diagnostics are available (e.g., $H\alpha$, CaII and MgII), from estimates of a column density and the projected cross-sectional area typical masses of $2\text{--}6 \times 10^{14}$ kg are recovered (see Dunstone *et al.* 2006).

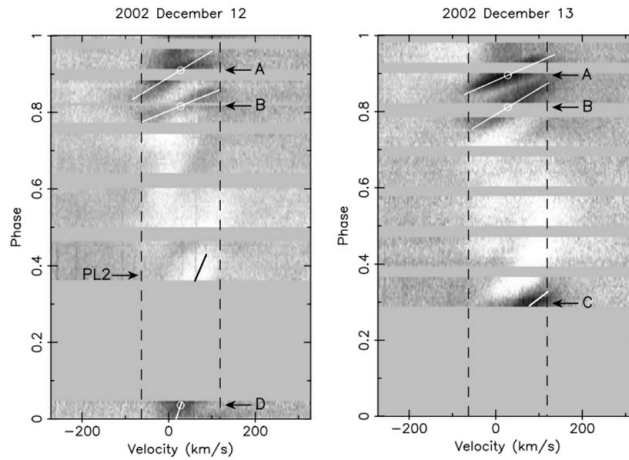


Figure 5. Time-series of H α spectra on the K0 dwarf, AB Dor (from Hussain *et al.* 2007). Clear transient features are seen moving from $-v_e \sin i$ to $+v_e \sin i$ (marked by the dashed vertical lines). These data were taken on consecutive nights and two prominence complexes are recovered at the same phase though with changing velocities, implying the heights changed within 1 day ($2P_{\text{rot}}$). The complex A moves out from 2.55 to $3.48R_*$ while the complex B moves in from 3.74 to $2.55R_*$. Given the stellar inclination angle of 60° these prominences must be at high latitudes in order to transit across the projected stellar disk.

Assuming the magnetic field confining the structures is rigid the rotation period of the cloud, and its rate of transit across the stellar disk indicates the distance of the “prominence” from the stellar rotation axis (also see Collier Cameron & Robinson 1989):

$$v_a(t) = d_a v_e \sin i \cos l \sin \frac{2\pi t}{P_{\text{rot}}} \quad (5.1)$$

where v_a is the velocity of the absorption transient, d_a is the height of the absorption transient in stellar radii, l is the latitude and P_{rot} is the rotation period of the star. By measuring the slope of the transient it is therefore possible to derive the longitude and height of each cloud causing the transient. Occasionally there is structure in these transients so it is only possible to determine the mean velocity of the larger complex.

The exact nature of these prominence type complexes has been a subject of debate but there is evidence from other diagnostics that active cool stars can support stable structures several stellar radii above the stellar surface. UV spectra of the binary system, V471 Tau (DA+K2V, $P_{\text{rot}} = 0.52\text{d}$) indicate the presence of discrete structures above $2R_*$ as absorption in various chromospheric lines with temperatures between 8000 to 10^4 K (Walter *et al.* 2004). Radio observations also imply the presence of extended coronae in M stars (Alef *et al.* 1997).

5.1. Mass ejections

Very few stars have been as intensely monitored with dense spectroscopic time-series as the K0 star, AB Dor. Over a re-examination of data acquired almost annually over a decade only three possible ejection events have been identified (Fig. 6).

Leitzinger *et al.* (2011) report evidence for an ejection event in the low mass star, AD Leo (M4.5V, $P_{\text{rot}} = 2.24\text{d}$) as indicated by enhanced blue-shifted emission in the transition line OVI 1032Å (Fig. 7). The velocity measured for this event would correspond to a distance of almost $28R_*$, i.e., well outside the $11.7R_*$ Keplerian corotation radius and supporting the interpretation of an ejection event. Studies are currently underway

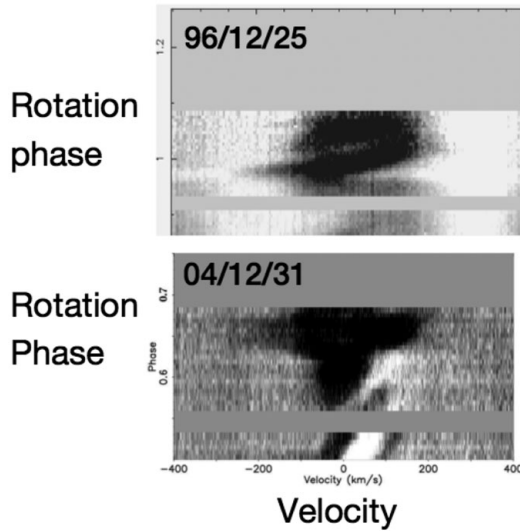


Figure 6. Observations of blue-shifts associated with absorption transients, indicating that part of the cool absorbing cloud is being ejected, reaching velocities of up to -180 km/s (Donati *et al.* 1997, Dunstone 2008). Only three such events have been found despite intense spectroscopic monitoring of this system, AB Dor, over 3-5 night observing runs every 1-2 years for 20 years. Ejection events such as these are difficult to observe without intense monitoring as they only last 15-20 minutes.

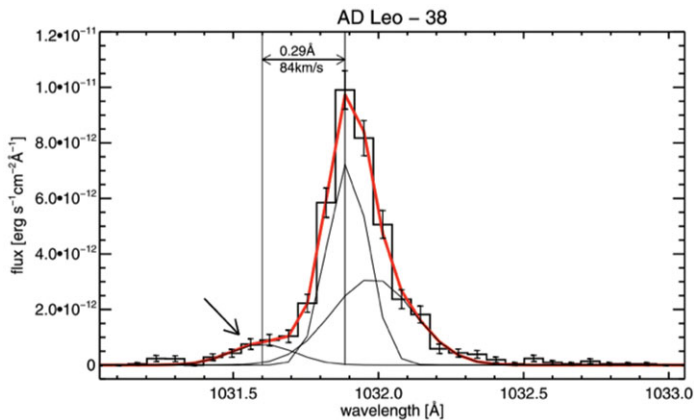


Figure 7. An enhancement in the blue-wing of the OVI 1032\AA line of the M star AD Leo following a flare event (Leitzinger *et al.* 2011). This indicates a velocity shift of -84 km s^{-1} and is likely caused by an ejection vent.

that are following this up on a larger sample of stars to get better statistics on how often these events occur.

5.2. Coronal streamer model

Any model to explain the nature of these large-scale structures must explain how they can be stable out to several stellar radii. The evidence from X-ray and EUV data suggests that the closed corona must be relatively compact. Magnetic field maps of the surfaces of these active stars reveal complex, multipolar fields that must drop off quickly with height (as opposed to simple dipole fields) and are therefore unlikely to support a closed corona beyond $0.5R_*$. Jardine & van Ballegoijen (2005) propose that these stellar prominences

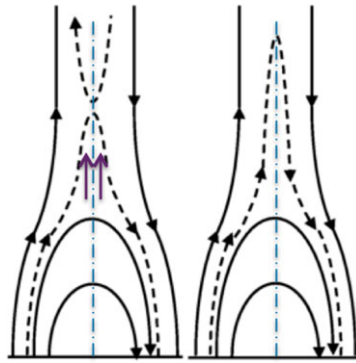


Figure 8. A schematic diagram showing how cool condensations may form above helmet streamers (adapted from Jardine & van Ballegoijen (2005)). Reconnection within the helmet streamer causes a closed loop to form (left). The stellar wind continues to act (arrows), which increases the density at the top of this loop. Radiative losses cool the loop and the internal pressure causes a new equilibrium (right). This implies that for a particular stellar magnetic field distribution there will be preferred longitudes at which these condensations continuously form above the neutral polarity lines (dot-dashed blue vertical line).

could be supported in the open field. Cool static equilibria can be found above coronal helmet streamers (Fig. 8). A clear prediction from this model is that prominences should be found above neutral polarity lines. This can now be tested with spectro-polarimetric studies of cool stars as the same datasets can be used to reconstruct the surface magnetic field and ascertain the positions of the prominences. Prominence positions and heights can be measured and used to predict the locations of neutral polarity lines that can be tested against the magnetic field maps reconstructed from the photospheric circularly polarised profiles.

6. Summary & Conclusions

While hot plasma appears confined to well within $0.5R_*$, particularly in G and K stars there is evidence of extended cooler structures with temperature ranging from 1000 to 10^4K from a variety of diagnostics, ranging from Balmer lines, to UV to radio wavelengths. There is also some evidence, though better statistics are needed, that the sizes of flaring loops change with spectral type, with increasing loop lengths found in late K and M-type stars. In contrast the prominence properties don't appear to change significantly with spectral type though stars with similar spectral types can host prominences that range from several stellar radii (up to $5R_*$) to very compact structures that appear much closer to the stellar surface. The model that can best explain the presence of these extended structures demonstrates that static equilibria can exist above neutral polarity lines with prominences forming above coronal helmet streamers, i.e., in the open field. This model can explain why prominences are often found at similar phases but different heights, implying that they are constantly being formed and ejected at preferential points related to the positions of neutral polarity lines in the stellar magnetic field. Ejection events themselves are only rarely observed - they can last up to approximately 20 min and are therefore challenging without continuous observations. It is possible to search for these events in both time-series of Balmer line profiles and as enhancements in the blue wings of transition and chromospheric line profiles. Future studies will enable us to gather better statistics on the frequency of these events across a range of spectral types.

References

- Alef, W., Benz, A. O., & Güdel, M. 1997, *A&A*, 317, 707
- Barnes, J. R., Collier Cameron, A., Unruh, Y. C., Donati, J. F., & Hussain, G. A. J. 1998, *MNRAS*, 299, 904
- Brickhouse, N. S., Dupree, A. K., & Young, P. R. 2001, *ApJ*, 562, L75
- Byrne, P. B., Eibe, M. T., & Rolleston, W. R. J. 1996, *A&A*, 311, 651
- Collier Cameron, A. & Robinson, R. D. 1989, *MNRAS*, 236, 57
- Donati, J.-F. & Collier Cameron, A. 1997, *MNRAS*, 291, 658
- Donati, J.-F., Collier Cameron, A., Hussain, G. A. J., & Semel, M. 1999, *MNRAS*, 302, 437
- Dunstone, N. J. 2008, *PhD thesis*, University of St Andrews, UK
- Dunstone, N. J., Collier Cameron, A., Barnes, J. R., & Jardine, M. 2006, *MNRAS*, 373, 1308
- Gabriel, A. H. & Jordan, C. 1969, *MNRAS*, 145, 241
- Huenemoerder, D. P., Testa, P., & Buzasi, D. L. 2006, 650, 1119
- Hussain, G. A. J., Donati, J.-F., Collier Cameron, A., & Barnes, J. R. 2000, *MNRAS*, 318, 961
- Hussain, G. A. J., Jardine, M., Donati, J.-F., Brickhouse, N. S., Dunstone, N. J., Wood, K., Dupree, A. K., Collier Cameron, A., & Favata, F. 2007, *MNRAS*, 377, 1488
- Jardine, M. & van Ballegooijen, A. A. 2005, *MNRAS*, 361, 1173
- Jeffries, R. D. 1993, *MNRAS*, 262, 369
- Kochukhov, O., Mantere, M. J., Hackman, T., & Ilyin, I. 2013, *A&A*, 550, 84
- Leitzinger, M., Odert, P., Ribas, I., Hanslmeier, A., Lammer, H., Khodachenko, M. L., Zaqarashvalli, T. V., & Rucker, H. O. 2011, *A&A*, 536, A62
- Maehara, H., Shibayama, T., Notsu, S., Notsu, Y., Nagao, T., Kusaba, S., Honda, S., & Nogami, D., Shibata K. 2012, *Nature*, 485, 478
- Mullan, D. J., Mathioudakis, M., Bloomfield, D. S., & Christian, D. J. 2006, *ApJS*, 164, 173
- Ness, J.-U., Güdel, M., Schmitt, J. H. M. M., Audard, M., & Telleschi, A. 2004, *A&A*, 427, 667
- Semel, M. 1989, *A&A*, 225, 456
- Schmitt, J. H. M. M. & Favata, F. 1999, *Nature*, 401, 44
- Testa, P., Drake, J. J., & Peres, G. 2004, *ApJ*, 617, 508
- Walter, F. M. 2004, *AN*, 325, 241